Ceramics-Silikáty 66 (2), 137-147 (2022)
www.ceramics-silikaty.cz 10.13168/cs.2022.0008

EFFECT OF Al_2O_3-RO RATIO ON THE STRUCTURE AND PROPERTIES OF ALKALINE EARTH ALUMINOSILICATE GLASS BASED ON THE MOLECULAR DYNAMICS SIMULATION

SHENGYUN YANG*, SHENG LI**, GUOXUAN GU*, YI CAO***, YA QU*, FENGYANG ZHAO****, YUNLONG YUE*,#, JUNFENG KANG*,#

*School of Materials Science and Engineering, University of Jinan, Jinan 250022, China
**Qingyuan CSG new energy-saving materials Co. Ltd
***School of Information Science and Engineering, University of Jinan, Jinan 250022, China
****State Key Laboratory for New Technology of Float Glass, 751 Donghai Dadao, Bengbu, Anhui, China

#E-mail: zztg_yueyl@163.com, mse_kangjf@ujn.edu.cn

Submitted December 28, 2021; accepted February 14, 2022

Keywords: Molecular dynamics simulation, Glass melts, High-temperature viscosity, Micro-structure characteristics, Degree of network polymerisation

The molecular dynamics (MD) simulation method was used to study the influence of the Al_2O_3-RO (R = Ca, Mg) ratio on the structure and properties of CaO-MgO-Al_2O_3-SiO_2-Na_2O glass at high temperatures. The micro-structure characteristics, degree of network polymerisation (DNP), and high-temperature viscosity of the glass melts were analysed. The results showed that the coordination number of Si^{4+} and Al^{3+} remained about 4 in the process of replacing Al_2O_3 with RO. The silicon-oxygen and aluminium-oxygen tetrahedron content showed a decreasing trend with a decrease in the Al_2O_3 content, the bridging oxygen content decreased, and the degree of the network polymerisation of the glass decreased from 3.33 to 2.79. The decrease in the Al_2O_3 content also caused a rapid decrease in the glass fibre-forming temperature from 1637.66 K to 1552.87 K. According to the molecular dynamics calculation, the linear relationship between the DNP and fibre-forming temperature was obtained.

INTRODUCTION

High-performance glass fibre has the advantages of high specific strength, high temperature resistance, corrosion resistance, etc., and is widely used in the aerospace, automotive lightweight, and wind energy industries [1, 2]. High-performance glass fibre is mainly based on alkaline earth aluminosilicate glass system, including CaO-MgO-Al_2O_3-SiO_2-Na_2O (CMASN) glass systems, which has good chemical stability, electrical insulation, mechanical properties, and a low thermal expansion coefficient. However, due to the special composition, the high-temperature viscosity of CMASN glass is high, and correspondingly, the melting temperature is high. The structure of the glass determines the change in the viscosity of the glass melt with the temperature, and the main factor determining the change in the glass structure is the various oxides content [3, 4].

Up to now, the structure of CMASN glass has been systematically studied through experiments. Many researchers have also established a connection between the properties of the glass and its composition, and there are many studies on optimising the properties of CMASN glass by adjusting the composition of the glass. Tobias K. Bechgaard et al. [5] used Raman spectroscopy to study the effect of the MgO/CaO ratio on the structure of sodium aluminosilicate glass. Al had a vital influence on the structure and performance of the glasses. In glasses with a lower Al_2O_3 content, Mg was more likely to violate the Al avoidance rule than Ca. Sun Young Park et al. [6] used high-resolution solid-state nuclear magnetic resonance (NMR) to study the effects of different compositions on $Ca_2Al_2SiO_7$-$Ca_2MgSi_2O_7$ glass. The results showed that the partially decomposed Ca-O-Si was observed in all the glasses, which confirmed the non-random distribution of Ca^{2+} and Mg^{2+} around the bridging oxygen (BO) and non-bridging oxygen (NBO). Millena Lograd et al. [7] studied the relationship between the structure and properties of a series of alkaline earth aluminoborosilicate glasses composed of $60SiO_2$-$10Al_2O_3$-$10B_2O_3$-(20-x)$M_{(2)}O$-xM'O ($0 \le x \le 20$; M, M' = Mg, Ca, Sr, Ba, Na). The ^{27}Al NMR spectrum showed that the aluminium atoms in these glasses were four-coordinated. Solvang et al. [8] found that the viscosity of the glass melt containing only MgO in the high temperature zone and low temperature zone was lower than that of the glass melt containing only CaO. It indicated that Mg^{2+} in the glass made the degree of polymerisation of the network smaller and there were more broken bonds in the network. Yuanzheng Yue et al. [9] found that the brittleness of the glass melt reached the minimum value when Ca/(Ca+Mg) was

equal to 0.5, and the glass transition temperature also reached the minimum value. These changes reflected the "mixed alkaline earth effect".

However, most of these studies could only explain the change in the macroscopic properties with the composition, and it was difficult to explain the mechanism from a deeper perspective, that is, the change in the atomic structure with the composition. With the development of MD simulation technology, the further understanding of silicate glass will promote the exploration of the relationship between its composition, structure, and properties. Kejiang Li et al. [10, 11] found that the damage ability of MgO to the network structure was greater than that of CaO, and the viscosity in magnesium aluminosilicate systems was smaller. Shufang Ma et al. [12] studied the effect of FeO on CaO-MgO-SiO_2-Al_2O_3 glass by molecular dynamics simulation. The results suggested that FeO destroyed the network structure of the glass, increased the diffusion coefficient, decreased the viscosity, and decreased the degree of the network polymerisation.

To the best of our knowledge, there are few MD simulation studies on the relationship between the component and the high-temperature viscosity of molten CaO-MgO-Al_2O_3-SiO_2-Na_2O glass. At the same time, experiments under high temperature are dangerous and unstable, so this paper uses MD simulation to further study the influence of Al_2O_3/RO on the structure and properties of CMASN glass.

EXPERIMENTAL

Preparation and characterisation of samples

In this study, five compositions of alkaline earth aluminosilicate glass, named A-1, A-2, A-3, A-4 and A-5, have been chosen to present different types of glass networks as shown in Table 1. The mole fractions of SiO_2 and Na_2O were kept constant at 61 % and 1 %, and the selected raw material was the purity of Analytical Reagent. An appropriate amount of chemicals were taken and fully mixed in an agate mortar pestle, and then placed into a platinum crucible to melt them in a high-temperature resistance furnace to prepare the CMASN glass samples. After that, the mixture was melted for 4 h at about 1600 °C, and then quenched in water. The quenched glass was used for the high-temperature viscosity and density measurements.

Table 1. The chemical composition of the glass samples (mol. %).

Samples Number	SiO_2	Al_2O_3	CaO	MgO	Na_2O	Density ($g \cdot cm^{-3}$)
A-1	61	20	9	9	1	2.501
A-2	61	18	10	10	1	2.542
A-3	61	16	11	11	1	2.580
A-4	61	14	12	12	1	2.600
A-5	61	12	13	13	1	2.626

Glass viscosity is an important parameter for glass clarification, homogenisation, forming and filamentation. In the experimental part, the viscosity of the quenched glass was measured by an Orton RSV-1600 rotary high-temperature viscometer. The quenched glass (250 g) was placed in a platinum crucible, and the temperature was gradually raised to 1550 °C, then the cooling procedure was set and the data were recorded. The temperature range of the measurements was 1550 °C to 1150 °C, and the cooling rate was set to 2 $°C \cdot min^{-1}$. The relationship between the logarithm of the viscosity and the reciprocal of the temperature was fitted by Arrhenius [13] equation [14]:

$$ln\eta = lnA + \frac{B}{T} \quad (1)$$

Where lnA and B are the temperature-independent coefficients, T is the absolute temperature. According to the Arrhenius equation fitting, the corresponding viscosity (the viscosity is 100 Pa·s) of the glass at the fibre-forming temperature (T_{log3}) can be obtained.

Archimedes principle was used to measure the density of the glass. The glass sample was immersed in deionised water at room temperature (25 °C). Five samples for each glass were measured and the average density was calculated to reduce the error [15].

MD simulation approach

In order to explore the influence of Al_2O_3/RO on the micro-structure of the CMASN glass, five groups of glasses were designed. There were about 20,000 model atoms in each group. The size of the simulated box was determined by the number of atoms and the density of the glass. The density was the measured value of the glass sample produced in the experiment.

Lammps (Large-scale Atomic/Molecular Massively Parallel Simulator) package (Aug 16, 2019) was used in the MD simulation software in this paper [16, 17]. It was widely used in scientific research because it is an open source, free of charge SW with a rich force field and high computational efficiency. The choice of the potential function has a decisive effect on the success of the MD simulation. Each system has many potential parameters, and the simulation results could be different under the different potential parameters [18, 19]. The potential function used in this study of CMASN glass was the Born-Mayer-Huggins (BMH) potential [20]. The functional form of the BMH potential can be written as:

$$E_{(ij)} = \frac{q_i q_j}{4\pi\varepsilon_0 r_{ij}} + Aexp\left(\frac{\sigma - r_{ij}}{\rho}\right) - \frac{C}{r_{ij}^6} + \frac{D}{r_{ij}^8} \quad (r < r_c) \quad (2)$$

Where $E_{(ij)}$ is the sum of all the surrounding forces on each atom; the first term on the right side of the equation represents the long-range interaction Coulomb potential [21]; the second term is the short-range repulsive potential; the third and fourth terms are the van der Waals potential [22, 23]; q_i and q_j are the effective charge of atoms i and j, respectively; r_{ij} is the distance between atoms i and j; A, C, and D are all the energy parameters between the atoms; σ is an interaction-dependent length parameter; ρ is an ionic-pair dependent length parameter; r_c is the cut-off value. This calculation of the charge of each ion used a partial charge model to improve the calculation efficiency (q_{Si} = 1.89 eV, q_{Al} = 1.4175 eV, q_{Ca} = 0.945 eV, q_{Mg} = 0.975 eV, q_{Na} = 0.4725 eV, q_O = -0.945 eV), and the parameters used in the calculation were from Mutsui [24] and Jabraoui [25] as shown in Table 2.

In the MD simulation process, the Verlet algorithm was used to solve the classical mechanical equations [26], and the timestep is set to 1 fs. The long-range Coulomb interaction potential was calculated using the Ewald summation method, the accuracy was set to $1.0e^{-5}$, the cut-off distance was 10 Å, while the cut-off distance of the short-range BMH potential was set to 8.0 Å. At the same time, the Nose-Hoove method was used to control the temperature change [27]. The MD simulation process completely simulated the melting-cooling process of the glass under real conditions. First, a relaxation process of 30 ps was performed under 5000 K and the microcanonical ensemble (NVE) to form the random model of the system, and, at the same time, the stability and conservation of the system's energy were ensured. Then under the isobaric-isothermal ensemble (NPT), the glass was cooled from 5000 K to 300 K at the rate of 10 $K \cdot ps^{-1}$. During the cooling process, 30 ps canonical ensemble (NVT) and NVE relaxation were performed around the fibre-forming temperature of the glass, and the atomic motion trajectory file of the glass was the output. The atomic motion trajectory file was analysed by OVITO [28], VESTA [29], ISAACS [30], and other software. The micro-structure characteristics of the glass (including the pair distribution function between the ions in the glass [31], the coordination number of the network formers and network modifiers [27], the bond length and bond angle distribution between the ions [32], the bridge oxygen content in the glass [33, 34], the distribution of Q^n and the degree of the network polymerisation (DNP) of the glass [35, 36], etc. were provided by the MD simulation results.

RESULTS AND DISCUSSIONS

The change of viscosity

The relationship between the high-temperature viscosity and temperature of the glass with the different al-kalinity is shown in Figure 1. It can be seen from Figure 1a that the viscosity of all the glass samples decreased with an increase in the temperature and the viscosity of the glass melt decreased rapidly with a decrease in the Al_2O_3 content. The results were similar to those of Liang et al [37]. Figure 1b shows the relationship between the logarithm of the viscosity and the reciprocal of the temperature of the glass. It can be seen that there was a linear relationship between the logarithm of the viscosity of the glass melt and the reciprocal

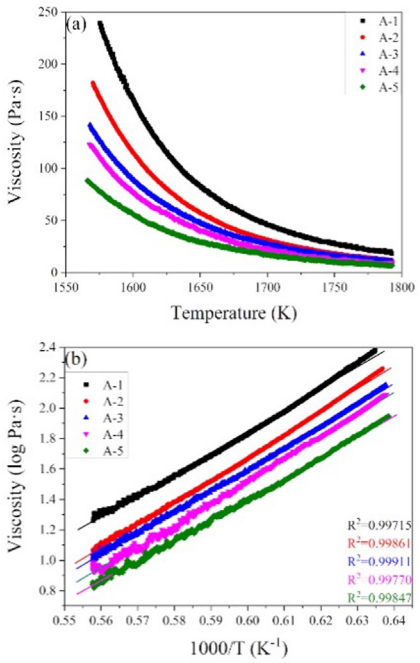

Figure 1. The relationship between the high-temperature viscosity and temperature of the glass (a) viscosity and temperature and (b) logarithm of the viscosity and reciprocal of the temperature.

Table 2. BMH potential function parameters.

Pairs	A (eV)	ρ (Å)	σ (Å)	C (eV·Å^6)	D (eV·Å^8)
Si-O	0.07719	0.167	2.9935	42.25	0
Al-O	0.08010	0.178	2.7155	27.28	0
Ca-O	0.07456	0.172	2.6067	34.57	0
Mg-O	0.06982	0.161	2.5419	46.29	0
Na-O	0.07612	0.180	2.9815	38.42	0
O-O	0.11967	0.276	3.6430	85.09	0

Table 3. The Arrhenius parameters *lnA* and *B*, the fibre-forming temperature (T_{log3}) of the glasses with the different alkalinity.

Samples	*lnA*	*B*	T_{log3} (K)
A-1	-6.58	14.06	1637.66
A-2	-7.48	15.28	1611.93
A-3	-6.77	13.96	1590.84
A-4	-7.21	14.55	1580.11
A-5	-6.77	13.62	1552.87

of the temperature. Therefore, the relationship between the viscosity and the temperature within the studied temperature range can be fitted by Arrhenius equation. Thus, the fibre-forming temperature (T_{log3}) of the glass can be obtained. Table 3 shows the fitting parameters and factors. It can be seen that the fibre-forming temperature of the glass samples decreased rapidly with a decrease in the Al_2O_3 content.

Local structure of the glass

The network structure of the CMASN glass under the different alkalinity obtained by the MD simulation is shown in Figure 2. It can be seen that the structure of the glass was connected by a three-dimensional network of [SiO_4] tetrahedrons (red) and [AlO_4] tetrahedrons (yellow). Ca (dark blue), Mg (light blue), and Na (green) filled in the gaps of the network structure [38, 39]. As Al_2O_3 was replaced by RO, the [AlO_4] tetrahedrons content in the glass decreased, and the structure of network was gradually filled with Mg and Ca.

Bond length and coordination number

The pair distribution function (PDF) showed the mutual distribution of the ions. The abscissa at the highest point of the first peak represented the bond length between the two ions, and the integral area corresponding to the first peak represented the first coordination number (CN) of the ion near the centre ion. The PDF and CN between the ions of the A-3 sample are shown in Figure 3. It can be observed in Figure 3a that, in the CMASN glass system, the bond length of Si-O, Al-O, Mg-O, Ca-O, Na-O and O-O were 1.66 Å, 1.77 Å, 2.06 Å, 2.48 Å, 2.55 Å, and 2.73 Å, respectively, which is consistent with the experimental results [40, 41]. The relationship between bond energy was completely opposite, the magnitude of the bond energy indicated the stability of the bond. It can be seen from Figure 3b that the CN of the silicon-oxygen was basically maintained at about 4, while the curve of the coordination number of the aluminium-oxygen was not as flat as that of the silicon-oxygen. This also meant the stability of the Al-O bond is obviously weaker than the Si-O bond [42].

The PDF between the different cations and oxygen

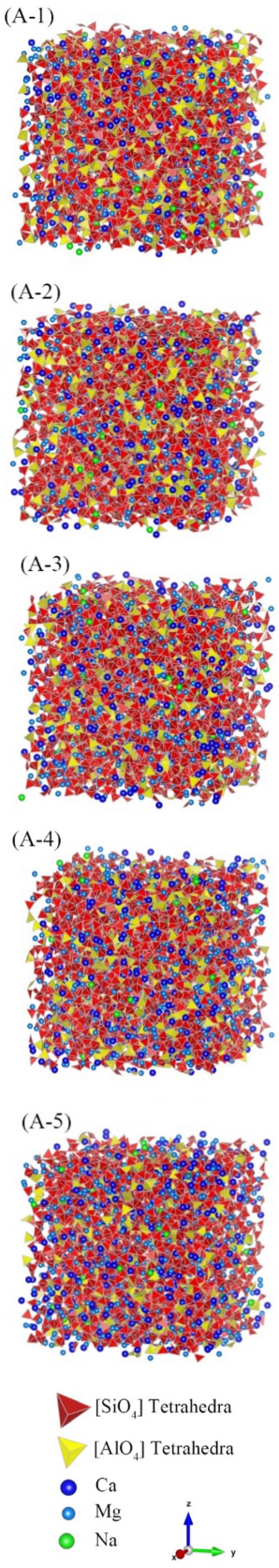

Figure 2. The network structure of the glass obtained by the MD simulation. [SiO_4] Tetrahedra (red), [AlO_4] Tetrahedra (yellow), Ca (dark blue), Mg (light blue), and Na (green).

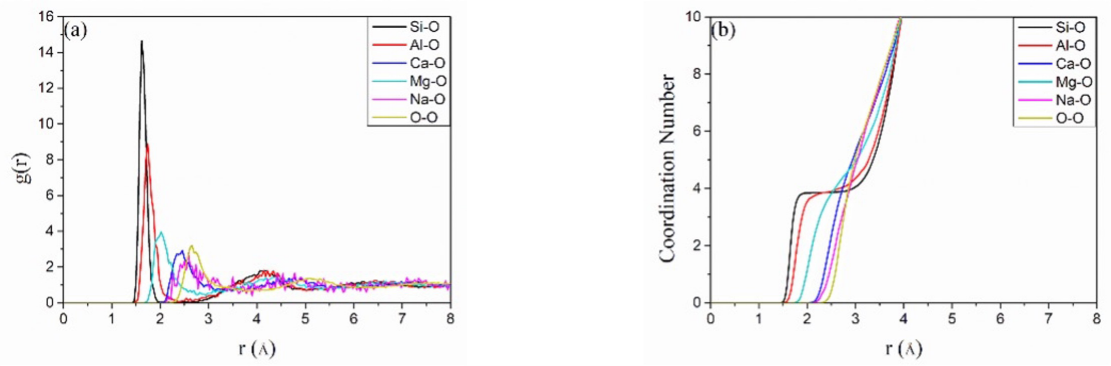

Figure 3. The (a) PDF and (b) CN of the A-3 sample.

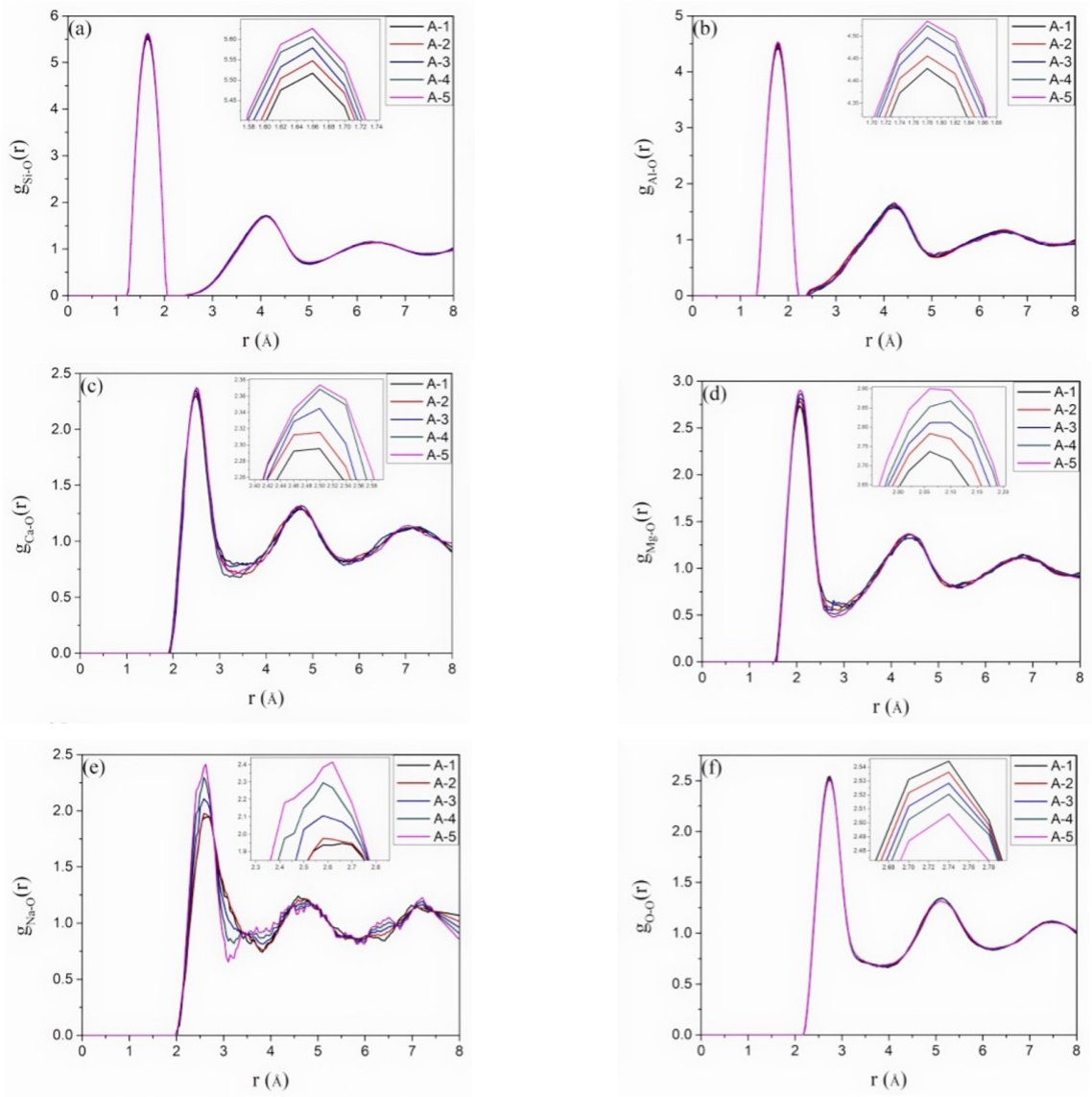

Figure 4. PDFs of (a) Si-O, (b) Al-O, (c) Ca-O, (d) Mg-O, (e) Na-O, and (f) O-O in the glasses with the different alkalinity.

ions are shown in Figure 4. It can be seen from Figure 4a that the bond length of the Si-O bond was around 1.66 Å and basically remained unchanged, which indicated that the Si-O bond and the structure of the silicon-oxygen polyhedral in the glass were always stable [18, 33]. As the skeleton of the most basic unit of the silicate glass, it did not change with the doping of the other network formers and modifiers. The bond length of the Al-O bond in Figure 4b was about 1.77 Å, which also did not change much with the composition. The span of the first peak of the Al-O bond was larger than that of the Si-O bond, which indicated that the strength of Al-O bond was weaker than the Si-O bond. The bond lengths of the Ca-O and Mg-O bonds in Figure 4c and d were around 2.48 Å and 2.06 Å, respectively, and the bond content increased with an increase in the RO. Due to the small Na_2O content in the glass, the curve shape of the Na-O bond in Figure 4e was disorganised. In Figure 4f, the O-O bond content gradually decreased as the RO content increased. The main reason was that more alkaline earth metal ions formed a coordination with the oxygen ions, which reduced the chance of oxygen-oxygen bonding.

The coordination number between the ions obtained by integrating the PDF is shown in Figure 5. It can be seen from Figure 5a that the coordination of Si^{4+} was around 4.0. It decreased as the RO content increased slightly, the platform of the image became wider [35]. In Figure 5b, the coordination number of Al^{3+} was slightly larger than that of Si^{4+}, and the width of the platform in the image was not as flat as that of Si^{4+}, which indicated that the stability of Al-O bonds was weaker than that of Si-O bonds [9]. The coordination number of Al^{3+} decreased with an increase in the RO content. It can be considered that excess alkaline earth metal ions destroyed the coordination of Al^{3+}. In Figures 5c and d,

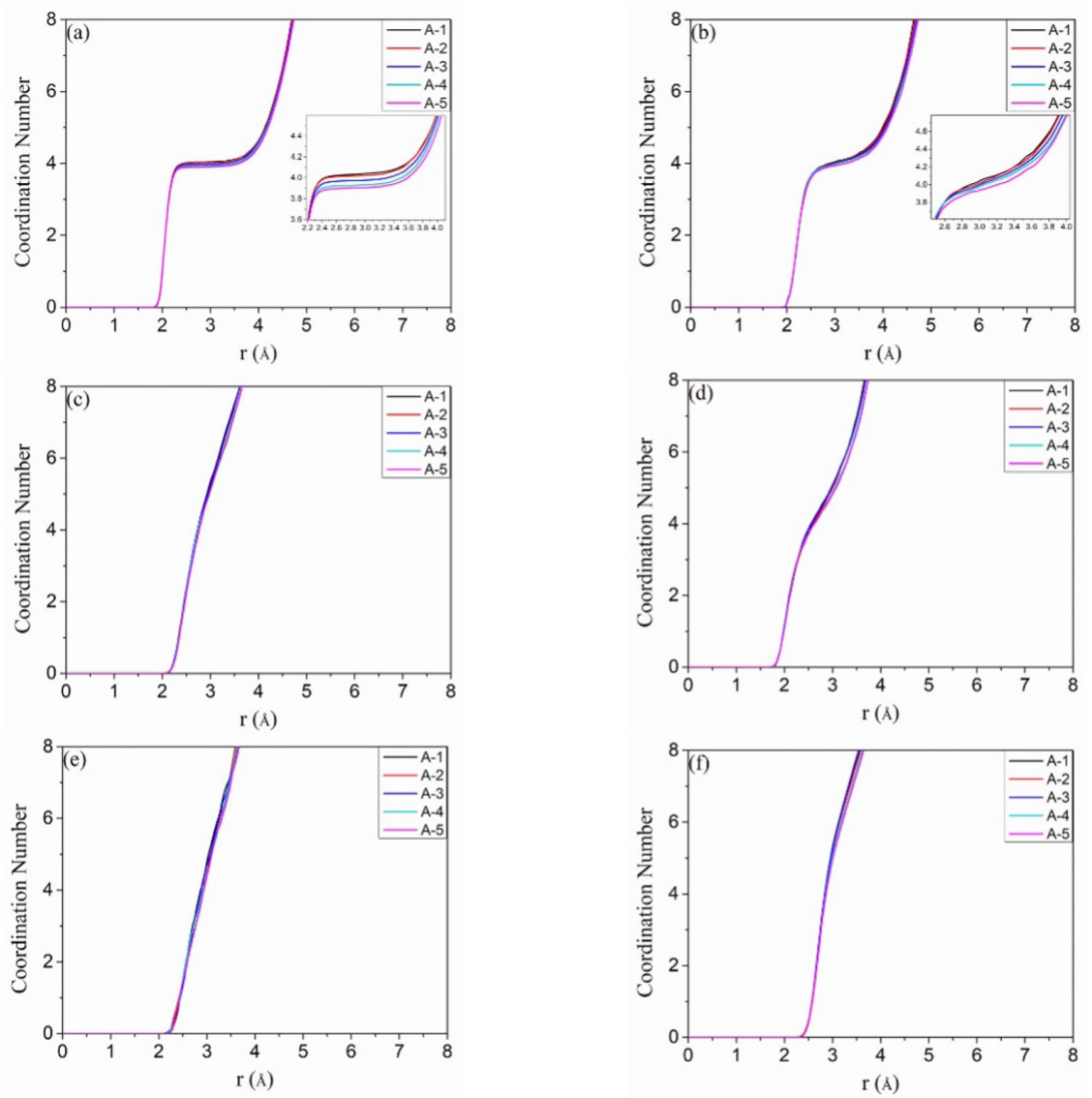

Figure 5. CNs of (a) Si-O, (b) Al-O, (c) Ca-O, (d) Mg-O, (e) Na-O, and (f) O-O in the glasses with the different alkalinity.

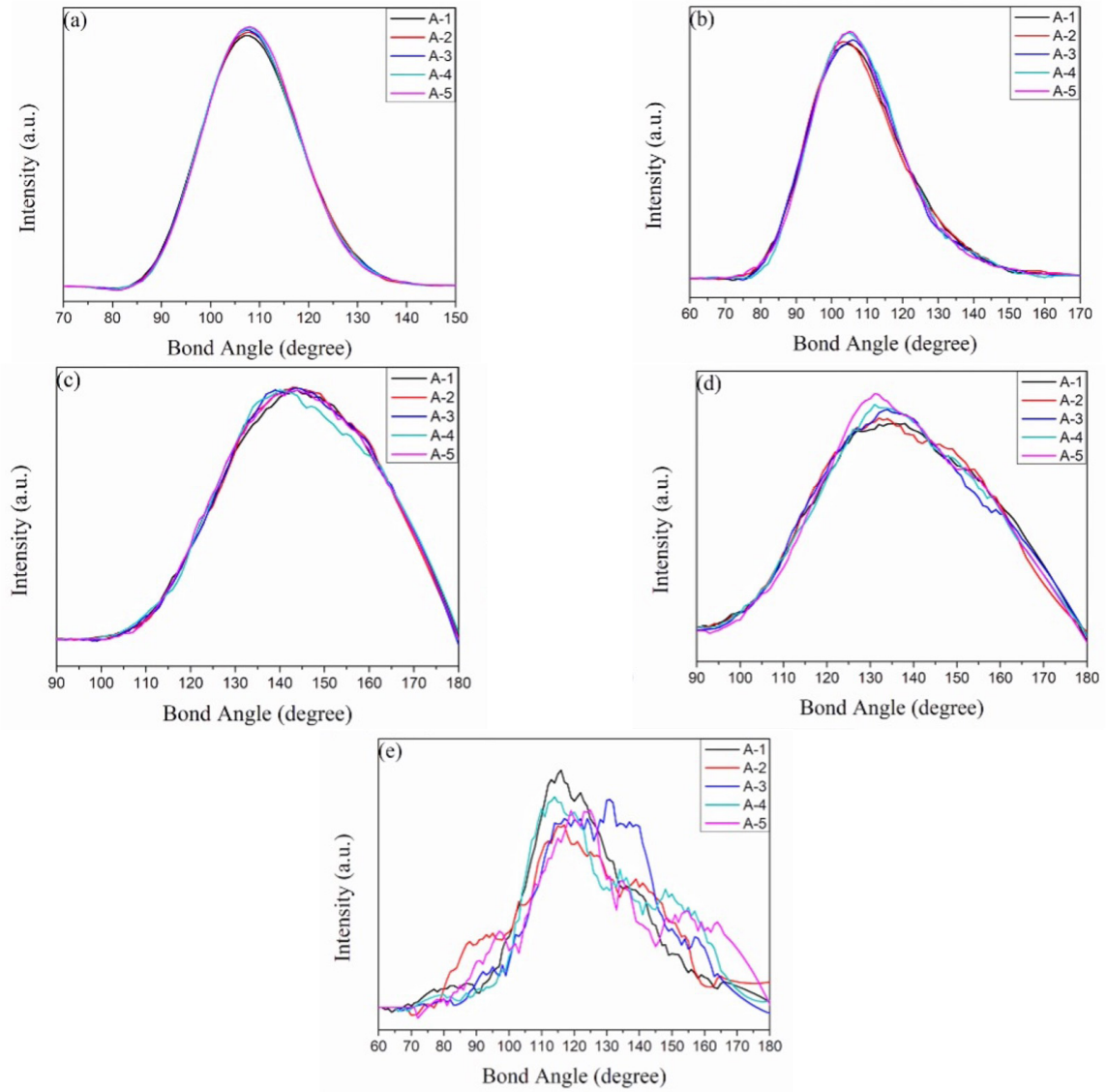

Figure 6. Bond angle distributions of (a) O-Si-O, (b) O-Al-O, (c) Si-O-Si, (d) Si-O-Al, and (e) Al-O-Al in the glasses with the different alkalinity.

the fluctuation of the coordination number of Ca^{2+} and Mg^{2+} was relatively large, and decreased with an increase in the RO. Among them, the coordination number of Ca^{2+} was larger, which also indicated that the stability of the Ca-O bond was lower than that of the Mg-O bond[10]. In Figure 5e, the Na^{+} coordination number did not have a stable platform, so the coordination between Na^{+} and O^{2-} was relatively divergent. In Figure 5f, there was no platform between O^{2-}, which showed a rather chaotic coordination state.

Distribution of bond angle

The angle between the ions in the glass network was an important parameter in the short-range structure. The distribution of the bond angles between the polyhedrons and within the polyhedrons in the CMASN structure of the glass are shown in Figure 6. The O-M-O (M = Si, Al) bond angle represented the angle within the tetrahedron in the glass, and its order degree represented the stability of the structure of tetrahedral. The centre of O-Si-O bond angle (Figure 6a) was 108°, which was very close to 109.5° of a standard tetrahedron. The O-Al-O bond angle (Figure 6b) was mainly concentrated at 105°, which was lower than that of O-Si-O. Moreover, the central bond angle decreased slightly, which indicated that the stability of $[AlO_4]$ was low. The M-O-M bond angle represented the degree of order between tetrahedrons in the glass. Figure 6c showed that the centre of Si-O-Si bond angle was about 142°, and the addition of RO had little effect on the angle of $[SiO_4]$ [43, 44]. As can be seen from Figure 6d, the decrease in the Si-O-Al bond angle indicated that the connection between $[SiO_4]$ and $[AlO_4]$ became weak. However, the disorder degree of the Al-O-Al bond angle in Figure 6e was mainly due to the aluminium avoidance effect between $[AlO_4]$.

Degree of network polymerisation of the glass

Distribution of BO and NBO

The bridging oxygen content in the glass is an important parameter to characterise the DNP of the structure of the glass. The BO refers to the oxygen with network forming ions connected at both ends. The change in the BO, NBO and free oxygen (FO) in the network structure of the CMASN glass with the different compositions are shown in Figure 7. As can be seen from Figure 7a, the BO was the main component in the silicon-oxygen network. With an increase in the RO content, the BO content decreased from about 68 % to about 54 %, the NBO content increased from about 31 % to about 43 %, and the FO content remained unchanged at about 2 %. Similarly, it can be seen from Figure 7b that the BO accounted for the main part in aluminium-oxide network, and the change trend in the BO, NBO and FO was the same as that in silicon-oxide network. This indicated that with the substitution of RO for Al_2O_3, the glass network became depolymerised and the connectivity decreased. It also suggested the destructive effect of RO on the medium range structure of the glass [21], which was similar to the experimental results of Sun et al [45].

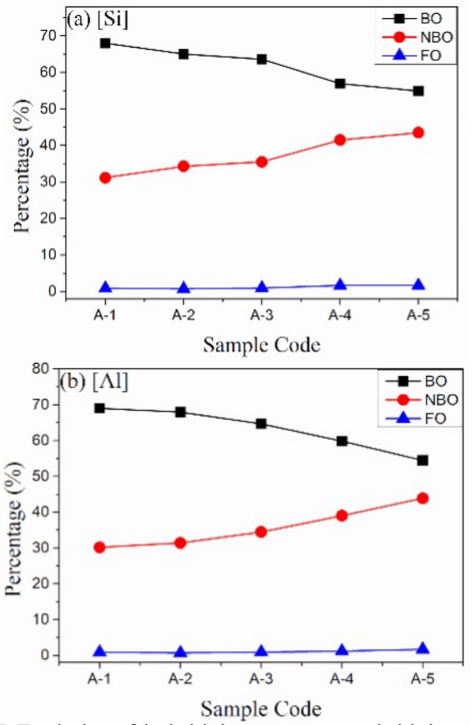

Figure 7. Evolution of the bridging oxygen, non-bridging oxygen, and free oxygen in the glasses with the different alkalinity, (a)Si, (b)Al.

Distribution of Q^n

The Q^n content in the structure of glass is another important parameter that characterises the DNP of the glass. Q represents the network forming body in the glass, and n (n = 0, 1, 2, 3, 4, 5) represents the number of BOs connected to the network forming body. The Q^n in the CMASN glass can be divided into Si-Q^n and Al-Q^n. The changes in the Q^n content in the glass network with the different alkalinity are shown in Figure 8. It can be seen from Figure 8a that an increase in the RO led to a significant decrease in the Si-Q^4 content, from 40 % to 21 %, the change of Si-Q^3 was relatively stable, between 41 % and 39 %, and the change of Si-Q^2 was opposite to that of Si-Q^4, from 15 % to 29 %. From the change in Q^4, Q^3, and Q^2 of Si, it suggested that with an increase in the RO, the excess free oxygen not only promoted the formation of [AlO_4], but also destroyed the network formed by [SiO_4]. This led to the transformation from Si-Q^4 to Q^3 and then to Q^2, and the silicon-oxygen network underwent the process of depolymerisation. Si-Q^1 increased from 1 % to about 8 % with an increase in the RO, Si-Q^0 fluctuated around 1 %. In Figure 8b, the main structures of the aluminium-oxygen network are still Q^4 and Q^3, which decreased from 60 % to 36 % and increased from 29 % to 41 % with an increase in the RO content, respectively. At the same time, Al-Q^2 increased from around 8 % to around 16 %, and Al-Q^1 also increased slightly. Al-Q^0 change very little, about 0.5%. This also suggested that the aluminium-oxygen network underwent depolymerisation during the process when the Al_2O_3 was replaced by the RO.

In order to better reflect the change in the structure of the glass, the DNP of the glass was characterised. The DNP of the glass is defined as [46]:

$$DNP = \sum_0^4 x_n * n \quad (3)$$

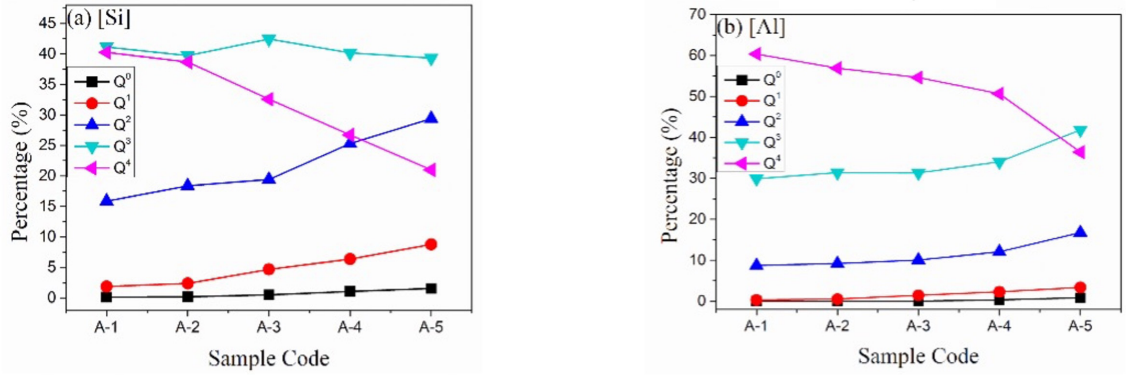

Figure 8. Evolution of Q^n in the glass network with the different alkalinity, (a)Si, (b)Al.

Where x_n is the content of Q^n, n = 0, 1, 2, 3, 4. The evolution of the DNP of the glass is shown in Figure 9. It can be seen from the figure that the change law of the glass network structure calculated by Q^n was the same as that discussed earlier. The increase in the RO content reduced the DNP of the glass from 3.33 to 2.79.

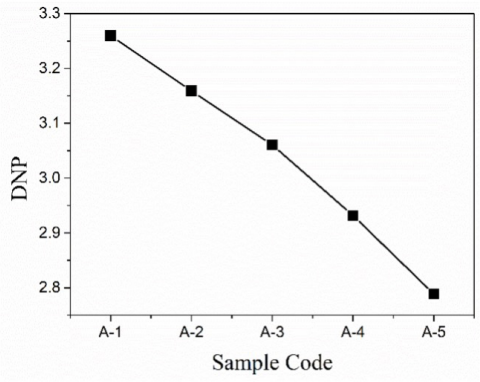

Figure 9. Evolution of the degree of the network polymerisation in the glasses with the different alkalinity.

Figure 10 shows the relationship between the DNP and the fibre-forming temperature (T_{log3}) of the glass when the viscosity was 100 Pa·s. The DNP and temperature showed a good linear relationship. It can be seen from the figure that the temperature increased with the increased DNP of the glass. This indicated that the DNP was the fundamental reason for the change in the glass temperature. Therefore, the temperature could be predicted by the DNP. The decrease in the Al_2O_3 content led to the gradual decrease in the BO content of the silicon-oxygen and aluminium-oxygen network, while it led to the increase in the NBO and FO content. In the glass network, Q^4 decreased when the RO content increased, while the Q^3 and Q^2 content significantly increased.

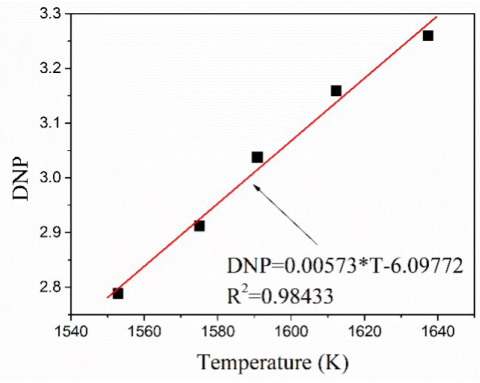

Figure 10. The relationship between the DNP and fibre-forming temperature in the glasses.

CONCLUSIONS

In this paper, the MD method was used to simulate the structural changes of the CMASN glass. The formula of five groups of glass samples was designed, and the effects of the Al_2O_3/RO ratio on the structure and properties of the glass were studied. The following conclusions were obtained: The coordination number of Si^{4+} and Al^{3+} remained about 4 in the process of replacing Al_2O_3 with RO. This was considered to be because the excess RO not only satisfied the coordination of Al^{3+}, but also the excess RO destroyed the ion coordination. The silicon-oxygen and aluminium-oxygen tetrahedron content showed a decreasing trend with a decrease in the Al_2O_3 content. The disorder of the Al-O-Al bond angle was mainly due to the aluminium avoidance effect between [AlO_4]. The BO content decreased, while the NBO and FO contents increased. The DNP of the glass decreased from 3.33 to 2.79. The decrease in the Al_2O_3 content also caused a rapid decrease in the glass fibre-forming temperature from 1637.66 K to 1552.87 K. According to the MD calculation, a linear relationship between the DNP and fibre-forming temperature was obtained. This indicated that a change in the Al_2O_3/RO ratio can affect the network structure of the glass. An increase in the RO content led to a decrease in the DNP of glass and the fibre forming temperature units.

Acknowledgment

This paper was funded by the National Natural Science Foundation of China (No. 51872117, No. 51804131, No. 52072148 and No. 51672105), the Natural Science Foundation of Shandong Province (No. ZR2019BEM002), and the Opening Project of the State Key Laboratory of Advanced Technology for Float Glass (No. 2020KF01).

REFERENCES

1. O' Higgins R. M., Mccarthy M. A., Mccarthy C T. (2008): Comparison of open hole tension characteristics of high strength glass and carbon fibre-reinforced composite materials. *Composites Science & Technology, 68*, (13), 2770-2778. Doi: 10.1016/j.compscitech.2008.06.003
2. Chen Z, Yu T, Park S J, et al. (2019): Rapid in situ remediation of glass fiber wind turbine blades in low temperature environment. *Modern Physics Letters B, 33*, 14-15. Doi: 10.1142/S0217984919400220
3. Korwin-EdSon M. L., Hofmann D. A., Mcginnis P. B. (2012): Strength of high performance glass reinforcement fiber. *International Journal of Applied Glass Science, 3*, (2), 107-121. Doi: 10.1111/j.2041-1294.2012.00089.x
4. Hong L., Richards C., Watson J. (2014): High-performance glass fiber development for composite applications. *International Journal of Applied Glass Science, 5*, (1), 65-

81. Doi: 10.1111/ijag.12053
5. Bechgaard T. K., Youngman et al. (2017): Structure of MgO/CaO sodium aluminosilicate glasses: Raman spectroscopy study. *Journal of Non-Crystalline Solids, 470*, 145-151. Doi: 10.1016/j.jnoncrysol.2017.05.014
6. Sun Y. P., Park C., Kim H. N., et al. (2020): Structure of type A CAI-like melts: A view from multi-nuclear NMR study of melilite ($Ca_2Al_2SiO_7$-$Ca_2MgSi_2O_7$) glasses. *Chemical Geology, 558*, 119894. Doi: 10.1016/j.chemgeo.2020.119894
7. Lograd M., Eckert H., Murata T., et al. (2021): Structure-property relations in crack resistant alkaline earth aluminoborosilicate glasses studied by solid state NMR. *Journal of the American Ceramic Society, 104* (5), 2250-2267. Doi: 10.1111/jace.17629
8. Solvang M., Yue Y. Z., Jensen S. L., et al. (2002): Rheological and thermodynamic response to compositional variation in high aluminosilicate melts. *Glassence & Technology, 75* (1), 465-468. Doi: 10.1023/A:1014205630938
9. Solvang M., Yue Y., Jensen S. L. (2004): The effects of Mg-Ca and Fe-Mg substitution on rheological and thermodynamic properties of aluminosilicate melts. *Journal of Non-Crystalline Solids, 345-346*, 782-786. Doi: 10.1016/j.jnoncrysol.2004.08.201
10. Jiang C., Li K., Zhang .J, et al. (2019): The effect of CaO and MgO on the structure and properties of coal ash in the blast furnace: A molecular dynamics simulation and thermodynamic calculation. *Chemical Engineering Science, 210*, 115226. Doi: 10.1016/j.ces.2019.115226
11. Jiang C., Li K., Zhang J., et al. (2018): The effect of CaO(MgO) on the structure and properties of aluminosilicate system by molecular dynamics simulation. *Journal of Molecular Liquids, 268*, 762-769. Doi: 10.1016/j.molliq.2018.07.123
12. Ma S.F., Li K.J., Zhang J.L., et al. (2021): Structural characteristics of CaO-SiO_2-Al_2O_3-FeO slag with various FeO contents based on molecular dynamics simulations. *JOM: the journal of the Minerals, Metals & Materials Society, 73* (6), 1637-1645. Doi: 10.1007/s11837-020-04511-y
13. Eyring H. (1936): Viscosity, plasticity, and diffusion as examples of absolute reaction rates. Eyring, H. (1936). Viscosity, plasticity, and diffusion as examples of absolute reaction rates. *The Journal of Chemical Physics, 4*(4), 283-291. Doi: 10.1063/1.1749836
14. Hrma P. (2008): Arrhenius model for high-temperature glass-viscosity with a constant pre-exponential factor. *Journal of Non-Crystalline Solids, 354* (18), 1962-1968. Doi: 10.1016/j.jnoncrysol.2007.11.016
15. Liu H.T., Li S., Wu F.N., et al. (2016): Effect of different Ca/La ratio on structure and properties of Al-B-Si glass with low dielectric constant. *Journal of Materials Science-Materials in Electronics, 27* (9), 9821-9827. Doi: 10.1007/s10854-016-5048-6
16. Plimpton S. (1995): Fast parallel algorithms for short-range molecular dynamics. *Journal of Computational Physics, 117* (1), 1-19. Doi: 10.1006/jcph.1995.1039
17. Crozier P. S. (2011). *LAMMPS molecular dynamics simulator*. https://www.lammps.org
18. Aoki H., Syono Y, Hemley R. J., et al. (2000). *Physics meets mineralogy: condensed matter physics in the geosciences.* UK: Cambridge University.
19. Allen M. P., Tildesley D. J. (2017): *Computer simulation of liquids*. 2nd ed., Oxford university press. Doi: 10.1093/oso/9780198803195.001.0001
20. Tosi M. P., Fumi F. G. (1964): Ionic sizes and born repulsive parameters in the NaCl-type alkali halides—II: The generalized Huggins-Mayer form. J*ournal of Physics and Chemistry of Solids, 25*(1), 45-52. Doi: 10.1016/0022-3697(64)90160-x
21. Bi Z.S., Li K.J., Jiang C.H., et al. (2021): Effects of amphoteric oxide (Al_2O_3 and B_2O_3) on the structure and properties of SiO_2-CaO melts by molecular dynamics simulation. *Journal of Non-Crystalline Solids, 559*, 120687. Doi: 10.1016/j.jnoncrysol.2021.120687
22. Massobrio C., Du J., Bernasconi M., et al. (2015). *Molecular dynamics simulations of disordered materials*. Springer. Doi: 10.1007/978-3-319-15675-0
23. Wang M.Y., Krishnan N.M.A., Wang B., et al. (2018): A new transferable interatomic potential for molecular dynamics simulations of borosilicate glasses. *Journal of Non-Crystalline Solids, 498*, 294-304. Doi: 10.1016/j.jnoncrysol.2018.04.063
24. Matsui M. (1994): A transferable interatomic potential model for crystals and melts in the system CaO-MgO-Al_2O_3-SiO_2. *Mineralogical Magazine, 58*, (2), 571-572. Doi: 10.1180/minmag.1994.58A.2.34
25. Hicham J., Michael B., Sébastien L., et al. (2018): Elastic and structural properties of low silica calcium aluminosilicate glasses from molecular dynamics simulations. *Journal of Non-Crystalline Solids, 499*, 142-152. Doi: 10.1016/j.jnoncrysol.2018.07.004
26. Verlet L. (1967): Computer 'experiments' on classical fluids. I. thermodynamical properties of Lennard-Jones molecules. *Health Physics, 22* (1), 79-85. Doi: 10.1097/00004032-197201000-00013
27. Lee J. G. (2011). *Computational Materials Science: An Introduction*. CRC.
28. Stukowski A. (2010): Visualization and analysis of atomistic simulation data with OVITO-the Open Visualization Tool. *Modelling & Simulation in Materials Science & Engineering, 18* (1), 2154-2162. Doi: 10.1088/0965-0393/18/1/015012
29. Momma K., Izumi F. (2011): VESTA3 for three-dimensional visualization of crystal, volumetric and morphology data. *Journal of Applied Crystallography, 44*, 1272-1276. Doi: 10.1107/S0021889811038970
30. Roux S. L., Petkov V., Le S. (2010): ISAACS-Interactive structure analysis of amorphous and crystalline systems. *Journal of Applied Crystallography, 43* (43), 181-185. Doi: 10.1107/S0021889809051929
31. Burgot J. L. (2017). *Radial Distribution Function*. Springer International Publishing. Doi: 10.1007/978-3-319-46401-5_29
32. Angeli F., Delaye J. M., Charpentier T., et al. (2000): Investigation of Al-O-Si bond angle in glass by 27Al 3Q-MAS NMR and molecular dynamics. *Chemical Physics Letters, 320* (5-6), 681-687. Doi: 10.1016/S0009-

2614(00)00277-3
33. Ren M.G., Deng L., Du J.C., (2017): Bulk, surface structures and properties of sodium borosilicate and boroaluminosilicate nuclear waste glasses from molecular dynamics simulations. J*ournal of Non-Crystalline Solids, 476*, 87-94. Doi: 10.1016/j.jnoncrysol.2017.09.030
34. Jakse N., Bouhadja M., Kozaily J., et al. (2012): Interplay between non-bridging oxygen, triclusters, and fivefold Al coordination in low silica content calcium aluminosilicate melts. *Applied Physics Letters, 101* (20), 251-158. Doi: 10.1063/1.4766920
35. Du J.C., Corrales L. R. (2006): Compositional dependence of the first sharp diffraction peaks in alkali silicate glasses: A molecular dynamics study. *Journal of Non-Crystalline Solids, 352* (30-31), 3255-3269. Doi: 10.1016/j.jnoncrysol.2006.05.025
36. Xiang Y., Du J.C., Smedskjaer M.M., Mauro J.C. (2013): Structure and properties of sodium aluminosilicate glasses from molecular dynamics simulations. *Journal of Chemical Physics, 139* (4), 87-148. Doi: 10.1063/1.4816378
37. Liang D., Yan Z.M., Lv X.W., et al. (2017): Transition of blast furnace slag from silicate-based to aluminate-based: structure evolution by molecular dynamics simulation and raman spectroscopy. *Metallurgical & Materials Transactions B, 48* (1), 573-581. Doi: 10.1007/s11663-016-0855-y
38. Sajid M., Bai C.G., Aamir M., et al. (2019): Understanding the structure and structural effects on the properties of blast furnace slag (BFS). *ISIJ International, 59* (7), 1153-1166. Doi: 10.2355/isijinternational.ISIJINT-2018-453
39. Le Losq C., Neuville D.R., Chen W.L., et al. (2017): Percolation channels: a universal idea to describe the atomic structure and dynamics of glasses and melts. *Scientific Reports, 7* (1). Doi: 10.1038/s41598-017-16741-3
40. Chojin K., Shimizu M,. Shimotsuma Y., et al. (2020): Cooling-rate dependence of thermal conductivity in a sodium silicate glass: A molecular dynamics study. *Journal of the Ceramic Society of Japan, 128*(9), 656-659. Doi: 10.2109/jcersj2.20039
41. Jiang C.H., Li K.J., Zhang J.L., et al. (2019): Molecular dynamics simulation on the effect of MgO/Al_2O_3 ratio on structure and properties of blast furnace slag under different basicity conditions. *Metallurgical & Materials Transactions B, 50* (1), 367-375. Doi: 10.1007/s11663-018-1450-1
42. Jiang C.H., Xiong Z.X., Bu Y.H., et al. (2020): Study on the structure and properties of high-Calcium coal ash in the high-temperature zone of a blast furnace: A molecular dynamics simulation investigation. *JOM, 72* (7), 2713-2720. Doi: 10.1007/s11837-020-04154-z
43. Du J.C., Cormack A.N. (2010): Molecular dynamics simulation of the structure and hydroxylation of silica glass surfaces. *Journal of the American Ceramic Society, 88* (9), 2532-2539. Doi: 10.1111/j.1551-2916.2005.00352.x
44. Geisinger K.L., Gibbs G.V., Navrotsky A. (1985): A molecular orbital study of bond length and angle variations in framework structures. Physics & Chemistry of Minerals, 11 (6), 266-283. Doi: 10.1007/BF00307405
45. Sun, Y.Q., Wang H., et al. (2018): Understanding the relationship between structure and thermophysical properties of $CaO\text{-}SiO_2\text{-}MgO\text{-}Al_2O_3$ molten slags. *Metallurgical & Materials Transactions B-Process Metallurgy & Materials Processing Science, 48* (2), 677-687. Doi: 10.1007/s11663-018-1178-y
46. Li ZH, He F, Zhang WT, et al. (2020): *Effect of Al_2O_3/SiO_2 on the structure and properties of blast furnace slag glass-ceramics*. Preliminary report. Doi: 10.21203/rs.3.rs-131872/v1